Propagation of acoustic waves in ducts with flow using the multimodal formulation

Bruno Mangin, Majd Daroukh, Gwénaël Gabard

Propagation of acoustic waves in ducts with flow using the multimodal formulation

Bruno Mangin*, Majd Daroukh†,
DAAA, ONERA, Paris Saclay University F-92322 Châtillon, France

Gwénaël Gabard‡
Acoustics Laboratory of the University of Le Mans (LAUM), UMR 6613, Institute of Acoustics - Graduate School (IA-GS), CNRS, Le Mans University, France

This paper presents a multimodal method for the computation of the acoustic field in an axisymmetric varying duct with or without liner and in the presence of mean flow. The original three-dimensional equations are rearranged into a set of coupled one-dimensional equations by projecting the acoustic field over transverse basis functions. To maintain the computational efficiency of the original multimodal method (applicable without flow), only the leading-order effects of the mean flow are modelled using a multiple-scales approach. A matching procedure is also given to deal with liner discontinuities in such a duct. Two different transverse bases are used: one is based on Fourier-Bessel functions to evaluate the effect of modal scattering and the other is based on Fourier-Chebyshev polynomials to improve the method efficiency. The formulation is evaluated against analytical models based on the Wentzel–Kramers–Brillouin technique and against finite-element solutions. It is shown to give consistent results for minor computational cost for modes propagating in ducts with or without acoustic liners. This method can be easily adapted to take into account more complex flows and geometries.

I. Introduction

Despite the development of analytical and numerical models for guided-wave problems, efficiently solving them remains a major challenge in turbomachinery for complex cases, such as critical reflections [1], cut-off waves [2].

Analytical methods have been developed to solve these guided wave problems in the case of constant ducts ([3], chapter 4, pp. 192-208) or in the case of varying ducts by introducing some simplifications on the geometry and the flow [4–8]. These studies take advantage of the fundamental aspect of in-duct acoustic propagation to separate the bounded transverse problem from the resolution in the axial propagation direction. They describe the solution as a transverse eigenmode multiplied by an axially varying amplitude, the shape of which is driven by a

Presented as Paper 2022-3098 at the 28th AIAA/CEAS Aeroacoustics Conference, Southampton, England, U.K., June 14–17, 2022;
*PhD student, Department of Aerodynamics, Aeroelasticity, and Aeroacoustics; bruno.mangin@onera.fr.
†Research Engineer, Department of Aerodynamics, Aeroelasticity, and Aeroacoustics; majd.daroukh@onera.fr.
‡Professor, Acoustics Laboratory of the University of Le Mans (LAUM); gwenael.gabard@univ-lemans.fr. Senior Member AIAA.

Wentzel–Kramers–Brillouin (WKB) ansatz. These methods provide fast results and allow a better understanding of the underlying physics. Despite their usefulness, they are not capable of predicting scattering phenomena caused by liner discontinuities or by changes in the duct geometry and flow. To overcome these difficulties, fully numerical simulations based on the linearized Euler equations or on the potential equation, such as the finite-element methods (FEM), can be used. Among them, commercial codes, like Actran-TM, which solves the potential equation (scalar equation) [9], are often chosen to solve this kind of propagation problems [10–12]. They allow to calculate precisely the solutions to these propagation problems, but they do not take fully advantage of the in-duct modal structure of the acoustic solution.

To do so it is possible to use an eigenmode decomposition in the transverse plane and to solve numerically the axial evolution of modes and their interaction. Several studies have been conducted with that idea (see for example [13, 14]) and demonstrate that the complexity comes from estimating the shape of the acoustic fluctuations in the axial direction. This idea is also the basis of the multimodal method (MM), which consists in rearranging the acoustic problem in a set of coupled one-dimensional (1D) equations describing the evolution of the mode amplitudes. However, two problems emerge when this method is used. First, the acoustic equation with evanescent modes is unstable, making it particularly difficult to solve. Then, the problem is not just an initial value problem since there is a strong coupling between the duct inlet and outlet. For two-dimensional (2D) ducts with varying cross-section, Pagneux *et al*. [15] overcame these difficulties by introducing an admittance matrix representing the medium's refraction and reflection index. They showed that the evolution of the admittance satisfies a Riccati equation which can be solved using a Magnus-Moebius scheme [16]. This method was then extended to curved ducts [17, 18] and proves to be fast and accurate. However, multimodal models have been restricted to solutions of the Helmholtz equation without mean flow.

The current paper extends this methodology to compute acoustic fields in axisymmetric ducts with potential mean flows. However, using an exact solution for the mean flow would significantly increase the complexity and calculation time of the method. This issue is addressed by using a simplified description of the flow, which is found using multiple-scales assumptions. This allows to account for the first-order effects of both convection and flow-induced scattering mechanisms, while maintaining the low calculation time of the standard multimodal formulation. The problem is solved by using Fourier series in the azimuthal direction and Chebyshev polynomials or Bessel functions in the radial direction to represent the perturbation variables.

The paper is organized as follows. In Section II, we provide a brief overview of the equations that govern the flow and acoustic fields, which serve as a basis to construct the proposed formulation. In Section III, the multimodal formulation with a multiple scales potential flow is developed, and the basis of transverse modes is defined. In Section IV, a matching procedure on the admittance is proposed to deal with impedance discontinuities. The developed method is then validated against analytical solutions in section V for an infinite uniform duct, and against FEM results and WKB results in section VI for a realistic engine geometry. Conclusions and discussions are provided in section VII.

II. Description of the problem

A. Governing equations

We consider the acoustic propagation inside a turbofan inlet represented by an axisymmetric waveguide with an axially slowly-varying annular cross-section, as shown in figure 1. Viscous and thermal effects are neglected. Vorticity is considered to be negligible, and no shock wave is expected. As a result, the flow is considered to be a perfect homentropic subsonic compressible irrotational gas flow. Note that it is quite common to use such a potential flow for aero-engine inlet ducts [4].

In the following, all the parameters are transformed to be dimensionless: densities are normalized by a reference density ρ_∞, velocities are normalized by a reference sound speed c_∞, spatial dimensions by the typical duct radius R_∞, velocity potentials by $R_\infty c_\infty$, and pressures by $\rho_\infty c_\infty^2$. We define the cylindrical coordinate system (x, r, θ) with the associated basis vectors $(\mathbf{e}_x, \mathbf{e}_r, \mathbf{e}_\theta)$, and the slowly-varying axial coordinate $X = \epsilon x$ where ϵ is a small parameter. The hub and tip radii are written $R_1(X)$ and $R_2(X)$, and their slow variations are defined as $\mathrm{d}R_1/\mathrm{d}x = \epsilon \mathrm{d}R_1/\mathrm{d}X + O(\epsilon^2)$ and $\mathrm{d}R_2/\mathrm{d}x = \epsilon \mathrm{d}R_2/\mathrm{d}X + O(\epsilon^2)$. The analysis is performed in the frequency domain and the angular frequency of the source ω is introduced. The velocity vector, density, speed of sound and pressure variables are written: $\tilde{\mathbf{v}} = \mathbf{V} + \mathrm{Re}(\mathbf{v}\, \mathrm{e}^{i\omega t}) = (U, V, W) + \mathrm{Re}((u, v, w)\, \mathrm{e}^{i\omega t})$, $\tilde{\rho} = D + \mathrm{Re}(\rho\, \mathrm{e}^{i\omega t})$, $\tilde{c} = C + \mathrm{Re}(c\, \mathrm{e}^{i\omega t})$, $\tilde{p} = P + \mathrm{Re}(p\, \mathrm{e}^{i\omega t})$ respectively. Capital letters denote time-averaged values, and lower-case letters represent unsteady harmonic perturbations. These notations are identical to those used by Rienstra [4].

In this framework, the steady Euler equations for the mean flow are:

$$\begin{aligned} \nabla \cdot (D\mathbf{V}) &= 0, \\ D(\mathbf{V} \cdot \nabla)\mathbf{V} &= -\nabla P, \\ C^2 = \frac{\gamma P}{D} &= D^{\gamma - 1}, \end{aligned} \tag{1}$$

where γ is the ratio of specific heats. For the perturbation variables, the linearized Euler equations are written:

$$\begin{aligned} i\omega\rho + \nabla \cdot (\rho\mathbf{V} + D\mathbf{v}) &= 0, \\ D(i\omega + \mathbf{V} \cdot \nabla)\mathbf{v} + D(\mathbf{v} \cdot \nabla)\mathbf{V} + \rho(\mathbf{V} \cdot \nabla)\mathbf{V} &= -\nabla p, \\ p = C^2\rho. & \end{aligned} \tag{2}$$

Hard-walled boundary conditions for the mean flow and lined wall boundary conditions for the acoustics (Myers

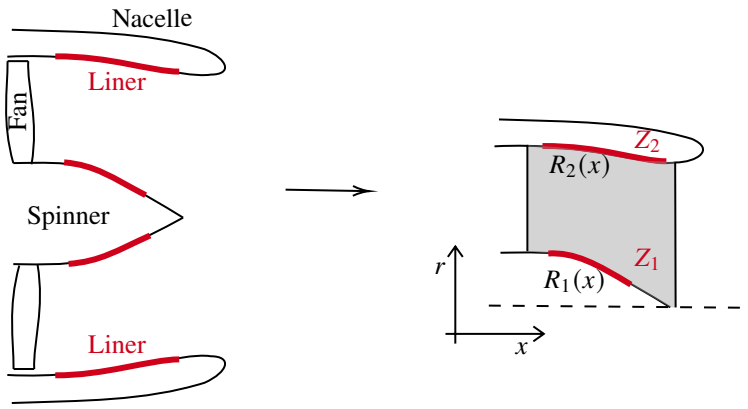

Fig. 1 Sketch of a generic turbofan and the associated wave-guide problem. The acoustic liner is shown in red, the dashed line corresponds to the axis of revolution and the computational area is filled in dark grey.

formulation [19]) are considered at the hub and tip. They write:

$$\begin{aligned} \mathbf{V}\cdot\mathbf{n}_i &= 0, \\ (\mathbf{v}\cdot\mathbf{n}_i) &= \frac{1}{\mathrm{i}\omega}(\mathrm{i}\omega + \mathbf{V}\cdot\nabla - \mathbf{n}_i\cdot(\mathbf{n}_i\cdot\nabla\mathbf{V}))\frac{p}{Z_i}, \end{aligned} \tag{3}$$

at $r = R_i(X)$, with $\mathbf{n}_i$ the unit outgoing vector normal to the surface, Z_i the impedance of the liner and $i = 1, 2$.

B. Base flow

Following Rienstra [4], the equations for the mean flow are solved by assuming that it varies slowly with the axial coordinate x. Noting that $\partial A/\partial x = \epsilon\partial A/\partial X + O(\epsilon^2)$ for any slowly-varying variable A, a reasoning on orders of magnitude then shows that the flow variables take the form:

$$\begin{aligned} \mathbf{V}(X, r; \epsilon) &= U_0(X)\mathbf{e}_x + \epsilon V_1(X, r)\mathbf{e}_r + O(\epsilon^2), \\ [D, P, C](X, r; \epsilon) &= [D_0, P_0, C_0](X) + O(\epsilon^2). \end{aligned} \tag{4}$$

Injecting these expressions into equation (1) gives:

$$\begin{aligned}
&\frac{1}{2}\left(\frac{F}{D_0(R_2^2-R_1^2)}\right)^2+\frac{1}{\gamma-1}D_0^{\gamma-1}=E+O(\epsilon^2),\\
&U_0=\frac{F}{D_0(R_2^2-R_1^2)}+O(\epsilon^2),\\
&P_0=\frac{1}{\gamma}D_0^{\gamma},\\
&C_0=D_0^{(\gamma-1)/2},\\
&V_1=V_1^a(X)r+V_1^b(X)\frac{1}{r}=-\frac{F}{2D_0}\frac{\partial}{\partial X}\left(\frac{1}{R_2^2-R_1^2}\right)r+\frac{F}{2D_0}\frac{\partial}{\partial X}\left(\frac{R_1^2}{R_2^2-R_1^2}\right)\frac{1}{r}+O(\epsilon),
\end{aligned} \tag{5}$$

where E and F are two constants (Bernoulli's constant and the cross-sectional mass flow rate, respectively). The numerical solution (e.g. calculated with a Newton algorithm) of the density's leading order D_0 allows to have access to the variation of all other mean flow quantities along the duct axis.

III. Multimodal formulation with a potential flow

A. Modified wave equation

In the standard multimodal formulation, the wave equation is solved using the acoustic pressure and axial velocity as primary variables. Solving the equation for pressure can be particularly complex in a case with flow, therefore we work here with the velocity potential ϕ such that $\mathbf{v}=\nabla\phi$. In the cylindrical coordinates, the velocity potential satisfies, from equations (2) and (3):

$$\nabla\cdot(D\nabla\phi)-D(i\omega+\mathbf{V}\cdot\nabla)\left[\frac{1}{C^2}(i\omega+\mathbf{V}\cdot\nabla)\phi\right]=0, \tag{6}$$

$$\mathrm{i}\omega(\nabla\phi\cdot\mathbf{n}_i)=-(\mathrm{i}\omega+\mathbf{V}\cdot\nabla-\mathbf{n}_i\cdot(\mathbf{n}_i\cdot\nabla\mathbf{V}))\left[\frac{D}{Z_i}(\mathrm{i}\omega+\mathbf{V}\cdot\nabla)\phi\right]\ \text{at } r=R_i(X)\ \text{with i}=1,2. \tag{7}$$

Using the flow expressions of equation (5) and keeping only the first-order terms yields:

$$\begin{aligned}
\frac{\partial}{\partial x}\left((1-M_0^2)u\right)=&\left(-\Delta_\perp-\left(\frac{\omega}{C_0}\right)^2-\frac{2\mathrm{i}\epsilon}{C_0^3}\frac{\mathrm{d}C_0}{\mathrm{d}X}\omega U_0+2\mathrm{i}\omega\frac{\epsilon V_1}{C_0^2}\frac{\partial}{\partial r}\right)\phi\\
&+\left(2\mathrm{i}\frac{\omega U_0}{C_0^2}+2\frac{\epsilon U_0V_1}{C_0^2}\frac{\partial}{\partial r}\right)u+O(\epsilon^2\omega^2U_0),
\end{aligned} \tag{8}$$

with $M_0(X)=U_0/C_0$ the axial Mach number, $\Delta_\perp$ the transverse Laplacian operator and $u=\dfrac{\partial\phi}{\partial x}$ the acoustic axial

velocity.* As for equation (7), it can be written:

$$\begin{aligned}\mathrm{i}\omega(\nabla\phi\cdot\mathbf{n}_i) = &-\left(-\omega^2\frac{D_0}{Z_i}+\mathrm{i}\omega U_0\epsilon\frac{\mathrm{d}}{\mathrm{d}X}\left(\frac{D_0}{Z_i}\right)+2\mathrm{i}\epsilon V_1\frac{D_0}{Z_i}\omega\frac{\partial}{\partial r}-\mathrm{i}\omega\frac{D_0}{Z_i}\frac{\partial\epsilon V_1}{\partial r}\right)\phi\\ &-\left(2\mathrm{i}\omega U_0\frac{D_0}{Z_i}+U_0\epsilon\frac{\mathrm{d}}{\mathrm{d}X}\left(\frac{D_0U_0}{Z_i}\right)+2\epsilon U_0V_1\frac{D_0}{Z_i}\frac{\partial}{\partial r}-\frac{D_0}{Z_i}\frac{\partial\epsilon V_1}{\partial r}U_0\right)u\\ &-\frac{D_0}{Z_i}U_0^2\frac{\partial u}{\partial x}+O(\epsilon^2\omega^2U_0).\end{aligned} \tag{9}$$

B. Multimodal approach

The next step consists in projecting the acoustic variables ϕ and u on linearly independent transverse cross-section functions so that the problem can be written as a set of first-order coupled differential equations. This basis is denoted $(\varphi_j)_{j\in\mathbb{N}}$, and the acoustic potential and its axial derivative write $\phi=\sum_j\phi_j(x)\varphi_j(X,r,\theta)$ and $u=\sum_j u_j(x)\varphi_j(X,r,\theta)$ respectively. Note that the basis is assumed to vary slowly in the axial direction.

Equation (8) is multiplied by a test function φ_i^*, chosen to be the complex conjugate of a basis function, and is integrated over the duct cross section S bounded by the boundary Λ. Then, by applying the divergence theorem, we obtain:

$$\begin{aligned}&\int_S\varphi_i^*\frac{\partial}{\partial x}\left((1-M_0^2)u\right)\mathrm{d}S=\\ &\int_S\left[\nabla_\perp\varphi_i^*\nabla_\perp\phi+\varphi_i^*\left(-k^2-\frac{2\mathrm{i}\epsilon}{C_0}\frac{\mathrm{d}C_0}{\mathrm{d}X}kM_0+2\mathrm{i}k\frac{\epsilon V_1}{C_0}\frac{\partial}{\partial r}\right)\phi+\varphi_i^*\left(2\mathrm{i}kM_0+2\frac{\epsilon V_1}{C_0}M_0\frac{\partial}{\partial r}\right)u\right]\mathrm{d}S\\ &-\int_\Lambda\varphi_i^*\nabla_\perp\phi\cdot\mathrm{d}\mathbf{\Lambda}+O(\epsilon^2\omega^2U_0),\end{aligned} \tag{10}$$

with $k=\omega/C_0$. The equation is transformed by using the mass conservation equation on the projection of ϕ and u over the basis $(\varphi_j)_{j\in\mathbb{N}}$ and becomes:

$$\begin{aligned}\frac{\mathrm{d}}{\mathrm{d}x}\left((1-M_0^2)\int_S\varphi_i^*\varphi_j dS u_j\right)=&\left[\int_S\nabla_\perp\varphi_i^*\nabla_\perp\varphi_j-k^2\varphi_i^*\varphi_j+\mathrm{i}k\epsilon\left(-M_0\left(\frac{1}{S}\frac{\mathrm{d}S}{\mathrm{d}X}+\frac{2}{C_0}\frac{\mathrm{d}C_0}{\mathrm{d}X}\right)\varphi_i^*\varphi_j\right.\right.\\ &-M_0\frac{\partial}{\partial X}(\varphi_i^*\varphi_j)+\frac{V_1}{C_0}\left(\varphi_i^*\frac{\partial}{\partial r}(\varphi_j)-\varphi_j\frac{\partial}{\partial r}(\varphi_i^*)\right)\mathrm{d}S+M_0\frac{\mathrm{d}}{\mathrm{d}X}\left(\int_S\varphi_i^*\varphi_j\mathrm{d}S\right)\Big)\Big]\phi_j\\ &+\left[\int_S 2\mathrm{i}kM_0\varphi_i^*\varphi_j+\epsilon\left(\frac{V_1M_0}{C_0}\left(\varphi_i^*\frac{\partial}{\partial r}(\varphi_j)-\varphi_j\frac{\partial}{\partial r}(\varphi_i^*)\right)-M_0^2\frac{1}{S}\frac{\mathrm{d}S}{\mathrm{d}X}\varphi_i^*\varphi_j\mathrm{d}S\right.\right.\\ &\left.\left.+(1-M_0^2)\frac{\partial}{\partial X}(\varphi_i^*)\varphi_j\right)\mathrm{d}S\right]u_j-\int_\Lambda\varphi_i^*\nabla\phi\cdot\mathrm{d}\mathbf{\Lambda}+O(\epsilon^2\omega^2U_0).\end{aligned} \tag{11}$$

When the acoustic boundary is hard-walled, $\int_\Lambda\varphi_i^*\nabla\phi\cdot\mathrm{d}\mathbf{\Lambda}=0$. Otherwise the equation (9) is injected into the previous equation. This leads to new equations governing the axial variation of the base function amplitudes $(\boldsymbol{\phi},\mathbf{u})=(\phi_j,u_j)_{j\in\mathbb{N}}$,

*The remaining terms are of order ϵ^2, but we want to highlight the mean flow velocity and the frequency scaling (valid for $\omega>1$).

which accounts for both the boundary conditions and the propagation operator:

$$\begin{pmatrix} A_{11} & 0 \\ 0 & A_{22} \end{pmatrix} \frac{\mathrm{d}}{\mathrm{d}x} \begin{pmatrix} \boldsymbol{\phi} \\ \mathbf{u} \end{pmatrix} = \begin{pmatrix} M_{11} & M_{12} \\ M_{21} & M_{22} \end{pmatrix} \begin{pmatrix} \boldsymbol{\phi} \\ \mathbf{u} \end{pmatrix} + O(\epsilon^2 \omega^2 U_0), \tag{12}$$

with:

$$\begin{aligned}
A_{11} &= M_{12} = (1 - M_0^2)\mathcal{A}, \\
A_{22} &= (1 - M_0^2)\mathcal{A} + \frac{\mathrm{i}D_0}{\omega} U_0^2 \mathcal{P}, \\
M_{11} &= -\epsilon(1 - M_0^2)\mathcal{B}, \\
M_{21} &= \mathcal{D} - k^2 \mathcal{A} + \mathrm{i}k\epsilon \left(-M_0 \left(\left(\frac{1}{S}\frac{\mathrm{d}S}{\mathrm{d}X} + \frac{2}{C_0}\frac{\mathrm{d}C_0}{\mathrm{d}X} \right) \mathcal{A} - \frac{\mathrm{d}}{\mathrm{d}X}(\mathcal{A}) \right) + ((C - C^*) - M_0(\mathcal{B} + \mathcal{B}^*)) \right) \\
&\quad - \frac{\mathrm{i}D_0}{\omega} \left(-\omega^2 \mathcal{P} + \epsilon \left(\mathrm{i}\frac{U_0}{D_0}\frac{\mathrm{d}D_0}{\mathrm{d}X}\omega\mathcal{P} + \mathrm{i}U_0\omega\mathcal{Q} + 2\mathrm{i}\omega\mathcal{R} - \mathrm{i}\omega\mathcal{S} \right) \right), \\
M_{22} &= 2\mathrm{i}kM_0\mathcal{A} + \epsilon \left((1 - M_0^2)\mathcal{B}^* - \frac{\mathrm{d}}{\mathrm{d}X}\left((1 - M_0^2)\mathcal{A} \right) + M_0(C - C^*) - \frac{M_0^2}{S}\frac{\mathrm{d}S}{\mathrm{d}X}\mathcal{A} \right) \\
&\quad - \frac{\mathrm{i}D_0}{\omega} \left(2\mathrm{i}\omega U_0 \mathcal{P} + \epsilon \left(U_0^2 \mathcal{T} - \frac{U_0^2}{S}\frac{\mathrm{d}(S)}{\mathrm{d}X}\mathcal{P} + U_0^2 \mathcal{Q} + 2U_0\mathcal{R} - U_0\mathcal{S} \right) \right),
\end{aligned} \tag{13}$$

and where * denotes the complex conjugate. The matrices $(\mathcal{A}, \mathcal{B}, C, \mathcal{D}, \mathcal{P}, \mathcal{Q}, \mathcal{R}, \mathcal{S}, \mathcal{T})$ are defined by:

$$\begin{aligned}
\mathcal{A}_{ij} &= \int_S \varphi_i^* \varphi_j \mathrm{d}S, \qquad \mathcal{B}_{ij} = \int_S \varphi_i^* \frac{\partial \varphi_j}{\partial X} \mathrm{d}S, \\
C_{ij} &= \int_S \frac{V_1}{C_0} \varphi_i^* \frac{\partial \varphi_j}{\partial r} \mathrm{d}S, \quad \mathcal{D}_{ij} = \int_S \nabla_\perp \varphi_i^* \nabla_\perp \varphi_j \mathrm{d}S, \\
\mathcal{P}_{ij} &= \int_0^{2\pi} \left(R_2/Z_2 \left. (\varphi_i^* \varphi_j) \right|_{r=R_2} + R_1/Z_1 \left. (\varphi_i^* \varphi_j) \right|_{r=R_1} \right) \mathrm{d}\theta, \\
\mathcal{Q}_{ij} &= \int_0^{2\pi} \left(R_2 \frac{\mathrm{d}[1/Z_2]}{\mathrm{d}X} \left. (\varphi_i^* \varphi_j) \right|_{r=R_2} + R_1 \frac{\mathrm{d}[1/Z_1]}{\mathrm{d}X} \left. (\varphi_i^* \varphi_j) \right|_{r=R_1} \right) \mathrm{d}\theta, \\
\mathcal{R}_{ij} &= \int_0^{2\pi} \left(R_2/Z_2 \left. \left(V_1 \varphi_i^* \frac{\partial \varphi_j}{\partial r} \right) \right|_{r=R_2} + R_1/Z_1 \left. \left(V_1 \varphi_i^* \frac{\partial \varphi_j}{\partial r} \right) \right|_{r=R_1} \right) \mathrm{d}\theta, \\
\mathcal{S}_{ij} &= \int_0^{2\pi} \left(R_2/Z_2 \left. \left(\frac{\partial V_1}{\partial r} \varphi_i^* \varphi_j \right) \right|_{r=R_2} + R_1/Z_1 \left. \left(\frac{\partial V_1}{\partial r} \varphi_i^* \varphi_j \right) \right|_{r=R_1} \right) \mathrm{d}\theta, \\
\mathcal{T}_{ij} &= \int_0^{2\pi} \left(R_2/Z_2 \left. \left(\varphi_i^* \frac{\partial \varphi_j}{\partial X} \right) \right|_{r=R_2} + R_1/Z_1 \left. \left(\varphi_i^* \frac{\partial \varphi_j}{\partial X} \right) \right|_{r=R_1} \right) \mathrm{d}\theta.
\end{aligned} \tag{14}$$

The matrices $(\mathcal{P}, \mathcal{Q}, \mathcal{R}, \mathcal{S}, \mathcal{T})$ are associated with the radial boundary conditions and characterize the attenuation due to the liner. In the case of a hard-walled duct, all these matrices are equal to zero.

It is important to note that the terms that have been neglected are scaled by $U_0\omega^2$. This means that the higher the

mean velocity and the frequency, the worse the expected results.

C. Admittance calculation

Equation (12) is unstable and cannot be integrated directly because of the presence of evanescent modes [1]. The multimodal method allows to solve this issue by defining an admittance matrix Y such that $\mathbf{u}(x) = Y(x)\boldsymbol{\phi}(x)$. This admittance links the acoustic potential and its axial derivative and is therefore representative of the reflection and refraction index of the medium (Poincaré–Steklov operator). This matrix is governed by a Riccati equation:

$$\frac{\mathrm{d}Y}{\mathrm{d}x} = -YA_{11}^{-1}M_{11} - YA_{11}^{-1}M_{12}Y + A_{22}^{-1}M_{21} + A_{22}^{-1}M_{22}Y + O(\epsilon^2\omega^2 U_0) \tag{15}$$

which is solved using a Magnus-Moebius scheme [1, 16] and an initial value Y_e.

One possibility to define the initial value is to consider a constant cross-section duct termination with only outgoing waves at the exit. In such a termination, all the global geometry and flow variables do not vary axially which implies that the admittance is a fixed point of the Riccati equation. To find this admittance, the acoustic variables are written using a summation of modes that propagate or decay exponentially with the axial distance:

$$\begin{pmatrix} \boldsymbol{\phi}(x) \\ \mathbf{u}(x) \end{pmatrix} = \sum_i \alpha_i \begin{pmatrix} \mathbf{w}_{i1} \\ \mathbf{w}_{i2} \end{pmatrix} e^{\mathrm{i}\lambda_i x}, \tag{16}$$

where $(\mathbf{w}_{i1}, \mathbf{w}_{i2})$ are the eigenvectors representing the weights associated with the distribution over the cross-sectional basis functions φ_i, λ_i are the associated axial wavenumbers and α_i are constants. By injecting the expression (16) into the propagation equation (12), by using the basis properties of the eigenvectors and by imposing that all the axial derivatives vanish, the following eigenvalue problem is obtained:

$$\mathrm{i}\lambda_i \begin{pmatrix} A_{11} & 0 \\ 0 & A_{22} \end{pmatrix} \begin{pmatrix} \mathbf{w}_{i1} \\ \mathbf{w}_{i2} \end{pmatrix} = \begin{pmatrix} 0 & M_{12} \\ M_{21} & M_{22} \end{pmatrix} \begin{pmatrix} \mathbf{w}_{i1} \\ \mathbf{w}_{i2} \end{pmatrix}, \tag{17}$$

with:

$$\begin{aligned} A_{11} &= M_{12} = (1 - M_0^2)\mathcal{A}, & M_{21} &= \mathcal{D} - k^2\mathcal{A} + \mathrm{i}D_0\omega\mathcal{P}, \\ A_{22} &= (1 - M_0^2)\mathcal{A} + \frac{\mathrm{i}D_0}{\omega}U_0^2\mathcal{P}, & M_{22} &= 2\mathrm{i}kM_0\mathcal{A} + 2D_0U_0\mathcal{P}. \end{aligned} \tag{18}$$

At the termination, only outgoing waves are propagating so that only the eigenvalues and eigenvectors associated to forward waves are kept. The propagation direction is given by the sign of $\mathrm{Re}(\lambda_i) - kM_0/(1 - M_0^2)$: if negative, the

wave goes forward; otherwise, it goes backward [4]. This allows to construct the forward matrix:

$$\begin{pmatrix} \boldsymbol{\phi}^+ \\ \mathbf{q}^+ \end{pmatrix} \propto \begin{pmatrix} W_1^+ \\ W_2^+ \end{pmatrix} e^{\Lambda^+ x}, \tag{19}$$

with $W_1^+ = (\mathbf{w}_{11}, ..., \mathbf{w}_{n1})$, $W_2^+ = (\mathbf{w}_{12}, ..., \mathbf{w}_{n2})$ and $\Lambda^+ = \mathrm{diag}(\mathrm{i}\lambda_1, ..., \mathrm{i}\lambda_n)$ and where $\lambda_1, ..., \lambda_n$ and $\mathbf{w}_{11}, \mathbf{w}_{12}, ..., \mathbf{w}_{n1}, \mathbf{w}_{n2}$ are the eigenvalues and eigenvectors associated to forward waves.

The resulting admittance matrix at the duct exit therefore writes:

$$Y_e = W_2^+ \left(W_1^+\right)^{-1} = W_1^+ \Lambda^+ \left(W_1^+\right)^{-1}. \tag{20}$$

D. Potential calculation

The admittance is calculated from the exit to the source by integrating the equation (15). Injecting the expression of the admittance into equation (12) gives us the following equation for the acoustic potential:

$$A_{11} \frac{\mathrm{d}}{\mathrm{d}x} (\boldsymbol{\phi}) = M_{11} \boldsymbol{\phi} + M_{12} Y \boldsymbol{\phi}. \tag{21}$$

It can then be calculated from the source to the exit given an initial value $\boldsymbol{\phi}_i$. Let us assume that we want to specify an incoming acoustic wave represented by its potential distribution $\boldsymbol{\phi}_i^+$. If no reflection is expected inside the duct, this can be the value kept for the imposed potential $\boldsymbol{\phi}_i$. Nevertheless, apart from rare cases, there are always waves travelling in the opposite direction, noted $\boldsymbol{\phi}_i^-$, due to geometrical or flow reflections.

Let us define the reflection matrix R such as $\boldsymbol{\phi}_i^- = R\boldsymbol{\phi}_i^+$. To obtain the reflection matrix R from the admittance matrix Y, the acoustic potential and its axial derivative are decomposed at the entry into a right and left propagating wave as:

$$\boldsymbol{\phi}_i = \boldsymbol{\phi}_i^+ + \boldsymbol{\phi}_i^- \text{ and } \mathbf{u}_i = \mathbf{u}_i^+ + \mathbf{u}_i^-. \tag{22}$$

Using the value of the admittance at the entrance and continuity conditions for the acoustic potential field and its axial derivative, the following relation is obtained:

$$Y(\boldsymbol{\phi}_i^+ + \boldsymbol{\phi}_i^-) = Y^+ \boldsymbol{\phi}_i^+ + Y^- \boldsymbol{\phi}_i^-, \tag{23}$$

with $Y^{+/-}$ corresponding to the admittance matrix associated to the waves propagating forwards or backwards at the entrance. Since the previous relation is true for any injected field $\boldsymbol{\phi}_i^+$, we obtain $R = (Y - Y^-)^{-1}(Y^+ - Y)$ and the forced potential is $(I_d + R)\boldsymbol{\phi}_i^+$, with I_d the identity matrix.

E. Transverse mode basis

If an arbitrary basis is chosen for φ_j, computing the matrices in equation (12) is time-consuming and the method would not bring a significant benefit compared to a fully numerical code. Therefore it is important to use a basis leading to analytical expressions for integrals in equation (14).

1. Standard hard-walled modes - Fourier-Bessel basis

Most multimodal studies [1, 15, 17, 20] use standard basis functions composed of local hard-walled transverse eigenmodes, solutions to the following eigenvalue problem:

$$-\Delta_\perp \varphi_j = \alpha^2 \varphi_j, \tag{24}$$

$$\frac{\partial \varphi_j}{\partial r} = 0 \text{ at } r = R_i(X) \text{ with } i = 1, 2. \tag{25}$$

For axisymmetric ducts, we associate a pair $(m, n) \in (\mathbb{Z}, \mathbb{N})$ to each index j such that the basis functions $\varphi_j = \varphi_{mn}$ are written [4]:

$$\varphi_{mn} = N_{mn} \left[\mathrm{J}_m(\alpha_{mn} r) + \Gamma_{mn} \mathrm{Y}_m(\alpha_{mn} r) \right] \mathrm{e}^{-\mathrm{i}m\theta}, \tag{26}$$

with m the azimuthal order, n the radial order, J_m and Y_m the m^{th}-order Bessel function of the first kind and second kind respectively and where the coefficient Γ_{mn} and the transverse eigenvalue α_{mn} can be found using the following relations:

$$\Gamma_{mn} = -\frac{\mathrm{J}'_m(\alpha_{mn} R_2)}{\mathrm{Y}'_m(\alpha_{mn} R_2)} = -\frac{\mathrm{J}'_m(\alpha_{mn} R_1)}{\mathrm{Y}'_m(\alpha_{mn} R_1)}. \tag{27}$$

The normalisation factor N_{mn} is chosen to be:

$$N_{mn} = \left(2\pi \int_{R_1}^{R_2} \left[\mathrm{J}_m(\alpha_{mn} r) + \Gamma_{mn} \mathrm{Y}_m(\alpha_{mn} r) \right]^2 r \mathrm{d}r \right)^{-0.5}. \tag{28}$$

As there is no possible coupling between different circumferential orders, we consider that the value of the azimuthal order m is fixed. In the following, no distinction is therefore made between j and n.

For a hard-walled duct, this basis has four major advantages:

1) analytical expressions for both $\mathcal{A}_{ij} = \delta_{ij}$ and $\mathcal{D}_{ij} = \alpha_i^2 \delta_{ij}$ are available,
2) it gives an analytical solution for the acoustic field in regions without scattering,
3) it is a complete basis, which means that any transverse shape can be recovered if a sufficient number of modes is used,
4) the matrix W_1^+ in equation (20) is the identity matrix and the admittance matrix is a diagonal matrix with the axial wavenumbers on the diagonal at the exit.

However, this basis presents a major weakness which leads to slow convergence for hardwalled ducts: the derivatives of all the basis functions are equal to zero at the wall, whereas the acoustic boundary condition (equation (3)) imposes a non-zero derivative for the potential gradient for a curved wall. Adding a non-physical supplementary Dirichlet mode inside the modal basis [18] allows to overcome this issue, but this is case-dependent.

The matrices $\mathcal{A}$ and $\mathcal{D}$ are diagonal and represent the propagation in the straight parts of the duct (isolated mode propagation). The matrices $\mathcal{B}$ and $\mathcal{C}$ have non-diagonal terms that are equal to zero only when there is no wall variationand can therefore be related to geometrical/flow scattering. The modal scattering can be artificially turned off by imposing that $\mathcal{B}$ and $\mathcal{C}$ are equal to zero. In this case, all the matrices are diagonal and the modes do not interact (the method can thus be referred to as multimodal without scattering).

It is worth noting that the multiple-scales approximation weakly impacts the self-propagation terms since the neglected terms ($O(\epsilon^2\omega^2 U_0)$) are flow-scattering terms.

2. Fourier-Chebyshev basis

To overcome the limitations of standard hard-walled modes which struggle to satisfy the wall boundary conditions, a new type of basis function is employed. A Fourier series again represents the acoustic field in the circumferential direction, while a set of Chebyshev polynomials is used in the radial direction to take advantage of their good convergence properties [7, 21, 22]. A first choice would be to take:

$$\varphi_j = \varphi_p^m = T_p\left(\frac{r - R_1}{R_2 - R_1}\right) e^{-\mathrm{i}m\theta}, \tag{29}$$

with T_p a shifted Chebyshev polynomial of the first kind of order $p \in \mathbb{N}$. However in the case of circular ducts ($R_1 = 0$), some integrals in the matrix D are not defined when $m \neq 0$ ($\lim_{\delta\to 0}\int_\delta^{R_2} r^{-1}\mathrm{d}r = \infty$). One solution is to replace R_1 by a small, non-zero value in the case of a circular duct, typically the spacing between two central collocation points. Due to the proprieties of the duct modes (behaviour as $r^{|m|}$ when $r \to 0$ [23]), this choice means the matrix D is poorly conditioned. A better solution would be to add a constraint on the coefficients of Fourier expansions to have basis functions of the form $rf(r)e^{-\mathrm{i}m\theta}$ when $m \neq 0$. We therefore choose, for all m:

$$\varphi_p^m = \left(\frac{r}{R_2 - R_1}\right)^{\min(|m|,1)} T_p\left(\frac{r - R_1}{R_2 - R_1}\right) e^{-\mathrm{i}m\theta}. \tag{30}$$

With this basis, the matrix D is well defined and the physical behaviour is better respected in the case of circular ducts. In addition, the expressions of the matrices given in equation (14) can be developed (see Appendix A) such that all the integrals that remain are independent of frequency, flow, geometry and azimuthal order, which is a major benefit of the chosen basis. These integrals only need to be computed once and can then be stored, thus allowing for fast computations.

Note that there is again no possible coupling between different circumferential Fourier modes. Therefore we consider that the value of the azimuthal order m is fixed, and, in the rest of the paper, no distinction is made between φ_p^m and φ_p. For convenience, this basis is called Chebyshev basis in the following.

IV. Impedance discontinuities

The equation (12) derived in the multimodal approach is valid as long as the impedance is represented by a differentiable function. However, in practice, the liner is only applied on a finite portion of the duct, which induces impedance discontinuities. They result in a non-defined matrix Q_{ij}, making the standard Magnus-Moebius scheme impossible to use. To solve this issue, several solutions are available. The first option is to impose a continuity of the acoustic potential and acoustic axial velocity (or the acoustic pressure and acoustic axial velocity) at both sides of a discontinuity, which is equivalent to impose a continuity of the admittance. The second option is to consider the duct as completely treated, but with an impedance that is regularized according to the axial coordinate. The third option is to use the conservation equations of mass and momentum to determine an admittance connection formula. The first option is incomplete, as it ignores reflections that occur at the axial location of the discontinuities [24]. The second option requires significant over-mesh of the "discontinuity" regions in order to correctly represent the rapidly varying impedance. In this paper, the third option is therefore preferred. The formula for the admittance across such a discontinuity is obtained in the following by deriving the admittance jump using the weak formulation of the acoustic equation over a vanishingly small control volume.

A. Formulation of the problem

The case of a slowly-varying duct with at least one impedance discontinuity, which can be located either on the hub or the tip, is studied. Let us consider one of these discontinuities, where the impedance varies from Z^- to Z^+, by defining a thin volume V that surrounds it. We assume that the impedance Z varies continuously from Z^- to Z^+ over a transition region of size 2δ, as sketched in figure 2. Note that the original problem is recovered when taking the limit $\delta \to 0$. The computational domain V is enclosed by the surfaces S_w, S_+, and S_-. S_+ and S_- are located respectively at $x = x_d + \delta$ and $x = x_d - \delta$, where x_d is the axial location of the discontinuity, and S_w corresponds to the duct wall surfaces. Finally, $\Lambda_\pm$ denote the contours along the perimeter of the duct at $x = x_d \pm \delta$.

B. Governing equations

Let us start by recalling the continuity equation and the mass equation for the perturbation variables:

$$\begin{aligned} \mathrm{i}\omega D\phi + D\mathbf{V}\cdot\nabla\phi + p = 0, \\ \nabla\cdot(D\nabla\phi) - D(\mathrm{i}\omega + \mathbf{V}\cdot\nabla)\left[\frac{1}{C^2}(\mathrm{i}\omega + \mathbf{V}\cdot\nabla)\phi\right] = 0. \end{aligned} \tag{31}$$

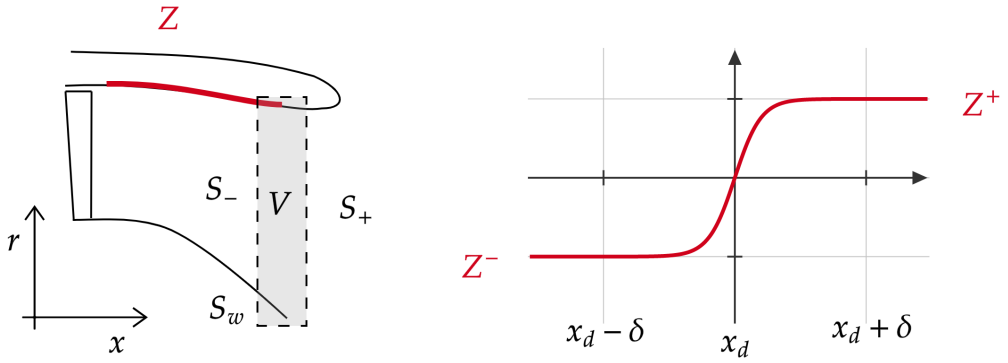

Fig. 2 Sketch of a generic liner discontinuity.

The weak formulation of these equations obtained through partial integration over the computational domain V writes:

$$\begin{aligned}\int_V \mathrm{i}\omega D\phi\varphi_i^* + D\mathbf{V}\cdot\nabla\phi\varphi_i^* + p\varphi_i^*\,\mathrm{d}V = 0,\\ \int_V \nabla\cdot(D\nabla\phi) - D(\mathrm{i}\omega + \mathbf{V}\cdot\nabla)\left[\frac{1}{C^2}(\mathrm{i}\omega + \mathbf{V}\cdot\nabla)\phi\right]\mathrm{d}V = 0,\end{aligned} \tag{32}$$

for a test function φ_i^* defined on V. The mass flow conservation, $\nabla\cdot D\mathbf{V} = 0$, is used to write $D\mathbf{V}\cdot\nabla\phi = \nabla\cdot\phi D\mathbf{V}$. Then, by applying the divergence theorem, it is straightforward to show that:

$$\begin{aligned}\int_V \mathrm{i}\omega D\phi\varphi_i^* - D\mathbf{V}\phi\cdot\nabla\varphi_i^* + p\varphi_i^*\,\mathrm{d}V = -\int_S D\mathbf{V}\phi\varphi_i^*\cdot\mathbf{n}\,\mathrm{d}S,\\ \int_V D\nabla\varphi_i^*\cdot\nabla\phi - \frac{D}{C^2}(\mathbf{V}\cdot\nabla\phi + \mathrm{i}\omega\phi)(\mathbf{V}\cdot\nabla\varphi_i^* - \mathrm{i}\omega\varphi_i^*)\,\mathrm{d}V = \int_S D\varphi_i^*\left(\nabla\phi - \frac{1}{C^2}(\mathbf{V}\cdot\nabla\phi + \mathrm{i}\omega\phi)\,\mathbf{V}\right)\cdot\mathbf{n}\,\mathrm{d}S,\end{aligned} \tag{33}$$

with $\mathbf{n}$ the unit outgoing normal vector. By reminding that a hard-walled boundary condition is used for the mean flow, $\mathbf{V}\cdot\mathbf{n} = 0$, the right-hand side of both equations can be developed as:

$$\begin{aligned}\int_S D\mathbf{V}\phi\varphi_i^*\cdot\mathbf{n}\,\mathrm{d}S = \int_{S+} DU\varphi_i^*\phi\,\mathrm{d}S - \int_{S-} DU\varphi_i^*\phi\,\mathrm{d}S,\\ \int_S D\varphi_i^*\left(\nabla\phi - \frac{1}{C^2}(\mathbf{V}\cdot\nabla\phi + \mathrm{i}\omega\phi)\,\mathbf{V}\right)\cdot\mathbf{n}\,\mathrm{d}S = \int_{S_w} D\varphi_i^*\frac{\partial\phi}{\partial n}\,\mathrm{d}S+\\ \int_{S+} D\varphi_i^* u\,\mathrm{d}S - \int_{S-} D\varphi_i^* u\,\mathrm{d}S + \int_{S-}\frac{UD}{C^2}(\mathbf{V}\cdot\nabla\phi + \mathrm{i}\omega\phi)\,\varphi_i^*\,\mathrm{d}S - \int_{S+}\frac{UD}{C^2}(\mathbf{V}\cdot\nabla\phi + \mathrm{i}\omega\phi)\,\varphi_i^*\,\mathrm{d}S.\end{aligned} \tag{34}$$

Further simplification can be done using Stokes' theorem to write (see Eversmann's paper [25] for more details):

$$\begin{aligned}\int_{S_w} D\varphi_i^* \frac{\partial \phi}{\partial n}\,\mathrm{d}S =& \frac{\mathrm{i}}{\omega}\int_{S_w} \frac{D^2}{Z}(\mathbf{V}\cdot\nabla\phi + \mathrm{i}\omega\phi)(\mathbf{V}\cdot\nabla\varphi_i^* - \mathrm{i}\omega\varphi_i^*)\,\mathrm{d}S + \\ & \frac{\mathrm{i}}{\omega}\int_{\Lambda_+} \frac{D^2}{Z}\left(\mathbf{V}\cdot\nabla\phi + \mathrm{i}\omega\phi\right)\varphi_i^*(\mathbf{n}\times\mathbf{V})\cdot\mathrm{d}\mathbf{\Lambda} + \frac{\mathrm{i}}{\omega}\int_{\Lambda_-} \frac{D^2}{Z}\left(\mathbf{V}\cdot\nabla\phi + \mathrm{i}\omega\phi\right)\varphi_i^*(\mathbf{n}\times\mathbf{V})\cdot\mathrm{d}\mathbf{\Lambda}.\end{aligned} \tag{35}$$

C. Matching procedure

To obtain a matching condition, we take the limit of the above expressions when $\delta \to 0$, which represents a liner discontinuity. We assume that the singularities of the acoustic potential axial derivative are finite, ensuring that the volume integrals of expression (33) vanish when the volume vanishes. By combining all of the previous equations, we obtain:

$$\begin{aligned}\int_{S+} DU\varphi_i^*\phi\,\mathrm{d}S - \int_{S-} DU\varphi_i^*\phi\,\mathrm{d}S = 0.& \\ \int_{S+} D(1-M^2)\varphi_i^* u\,\mathrm{d}S - \int_{S-} D(1-M^2)\varphi_i^* u\,\mathrm{d}S = \frac{\mathrm{i}}{\omega}\int_{\Lambda_+} \frac{D^2}{Z}\left(\mathbf{V}\cdot\nabla\phi + \mathrm{i}\omega\phi\right)\varphi_i^*(\mathbf{n}\times\mathbf{V})\cdot\mathrm{d}\mathbf{\Lambda}& \\ + \frac{\mathrm{i}}{\omega}\int_{\Lambda_-} \frac{D^2}{Z}\left(\mathbf{V}\cdot\nabla\phi + \mathrm{i}\omega\phi\right)\varphi_i^*(\mathbf{n}\times\mathbf{V})\cdot\mathrm{d}\mathbf{\Lambda}.&\end{aligned} \tag{36}$$

By reminding that the surface, the mean axial velocity and the mean density are continuous, the previous general equation show that the acoustic potential is continuous across the liner discontinuity. It also indicates that its axial derivative is not continuous if Z is not, which confirms that the admittance is not continuous across the discontinuity. To find its variation across the transition region, we project the velocity potential and its axial derivative over the basis $(\varphi_j)_{j\in\mathbb{N}}$. It yields:

$$\begin{aligned}\int_S D(1-M^2)\varphi_i^*\varphi_j \mathrm{d}S\left[\mathbf{u}^+ - \mathbf{u}^-\right] = \frac{\mathrm{i}}{\omega}\int_\Lambda \frac{D^2}{Z^+}\left(U\varphi_j\mathbf{u}^+ + \left(V\frac{\partial\varphi_j}{\partial r} + \mathrm{i}\omega\varphi_j\right)\boldsymbol{\phi}^+\right)\varphi_i^*(\mathbf{n}\times\mathbf{V})\cdot\mathrm{d}\mathbf{\Lambda}& \\ + \frac{\mathrm{i}}{\omega}\int_\Lambda \frac{D^2}{Z^-}\left(U\varphi_j\mathbf{u}^- + \left(V\frac{\partial\varphi_j}{\partial r} + \mathrm{i}\omega\varphi_j\right)\boldsymbol{\phi}^-\right)\varphi_i^*(\mathbf{n}\times\mathbf{V})\cdot\mathrm{d}\mathbf{\Lambda},&\end{aligned} \tag{37}$$

where $\boldsymbol{\phi}^\pm$ and $\mathbf{u}^\pm$ refer to the amplitudes of the acoustic potential and the acoustic axial velocity at $x_d \pm \delta$. By using the multiple-scales flow expressions of equation (5), this equation can be reduced to:

$$\begin{aligned}(1-M_0^2)\mathcal{A}(\mathbf{u}^+ - \mathbf{u}^-) = \frac{D_0U_0^2}{\mathrm{i}\omega}(\mathcal{P}^+\mathbf{u}^+ - \mathcal{P}^-\mathbf{u}^-) + & \\ \frac{D_0U_0}{\mathrm{i}\omega}(\mathrm{i}\omega\mathcal{P}^+\boldsymbol{\phi}^+ - \mathrm{i}\omega\mathcal{P}^-\boldsymbol{\phi}^- + \epsilon\left(\mathcal{R}^+\boldsymbol{\phi}^+ - \mathcal{R}^-\boldsymbol{\phi}^-\right)) + O(\epsilon^2\omega^2U_0),&\end{aligned} \tag{38}$$

where $\mathcal{A}, \mathcal{P}, \mathcal{R}$ are the matrices defined in section III. Finally, by writing $\mathbf{u}^+ = Y^+\boldsymbol{\phi}^+$ and $\mathbf{u}^- = Y^-\boldsymbol{\phi}^-$ the admittance

jump, $Y^- = \mathcal{L}(Y^+)$, across the impedance discontinuity can be found:

$$Y^- = \left(\left(1 - M_0^2\right)\mathcal{A} - \frac{D_0 U_0^2}{\mathrm{i}\omega}\mathcal{P}^-\right)^{-1} \left(\frac{D_0 U_0}{\mathrm{i}\omega}\left(\mathrm{i}\omega\mathcal{P}^- - \mathrm{i}\omega\mathcal{P}^+ + \epsilon\left(\mathcal{R}^- - \mathcal{R}^+\right)\right) + \left(\left(1 - M_0^2\right)\mathcal{A} - \frac{D_0 U_0^2}{\mathrm{i}\omega}\mathcal{P}^+\right) Y^+\right) + O(\epsilon^2\omega^2 U_0), \tag{39}$$

Note that the above expression shows that the admittance (and therefore the acoustic axial velocity) is continuous across the liner discontinuity when there is no mean flow.

V. Validation for an infinite uniform duct

For an infinite annular uniform duct with lined walls, the propagation problem reduces to the eigenvalue problem given in equation (17).

The resolution of this problem is checked for parameters representative of a modern engine inlet, with a unit nacelle radius R_2, a spinner radius R_1 equal to 0.3, a wall impedance Z_2 equal to $2 - \mathrm{i}$. The flow is uniform, D_0 and C_0 equal to 1 and M_0 equal to 0.5. The acoustic variables are computed at $\omega = 25$ and for an azimuthal mode $m = 24$ [26].

At first, both the distribution of the upstream eigenvalues in the complex plane and the shape of an upstream transverse function for the radial order $n = 5$ are computed using a Chebyshev basis, the results are plotted in figures 3a and 3b, to show the ability of this basis to correctly represents the duct modes. Excellent agreement is obtained when fifteen or twenty polynomials are used. However, with fewer polynomials, the solution quickly deteriorates, and with ten polynomials, the radial distribution of the mode is lost. When enough basis functions are used, there are only minor differences between the eigenvalues obtained numerically and the analytical ones. Note that this required number of basis functions is strongly dependent on the radial mode order.

Then, to evaluate the benefit of the Chebyshev basis over a standard hard-walled transverse basis, the reduction of the error with the increase of the number of basis functions is investigated using both bases. The evolution of the error on the radial eigenmode is defined by:

$$\epsilon_p = \left(\frac{\int |\phi_p - \phi_\infty|^2 r \mathrm{d}r}{\int |\phi_\infty|^2 r \mathrm{d}r}\right)^{1/2}, \tag{40}$$

with ϕ_p the potential obtained with p basis functions and ϕ_∞ the reference semi-analytical solution (computed as in [4]). The convergence of the Chebyshev and hard-walled Bessel bases is assessed in figure 3c. As expected, for a lined duct, the Chebyshev basis outperforms the Bessel basis when many polynomials are used, with an exponential error convergence rate. However, when few basis functions are used, the Bessel basis better represents the eigenmodes. These results confirm that the method has excellent convergence and accuracy if enough Chebyshev polynomials are used. As a rule of thumb, when $2n + 10$ polynomials are used, with n the highest radial mode order, the results are only weakly

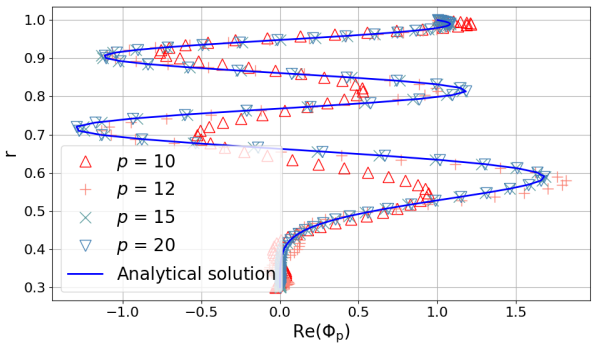

(a) Radial evolution of the eigenmode $n = 5$ (real part)

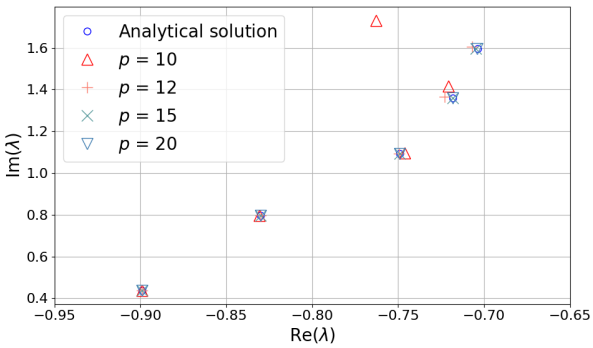

(b) First five radial computed eigenvalues in the complex plane

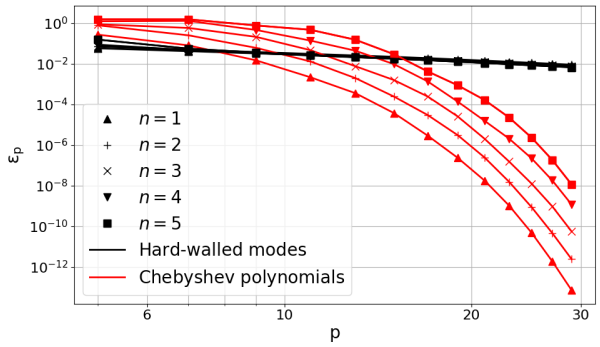

(c) Evolution of the error with the number of basis functions

Fig. 3 Validation of the eigenvalue resolution inside a constant waveguide with $(R_1, R_2) = (0.3, 1)$, $M_0 = 0.5$, $\omega = 25$, $m = 24$ and $Z_2 = 2 - \mathrm{i}$.

sensitive to the inclusion of further polynomials. This criterion is used in the remainder of the paper.

VI. Validation for a slowly-varying duct

A. Validation methodology

1. Test case geometry and flow conditions

For all the following test cases, a geometry representative of the CFM56 engine is used. We consider the engine to be axisymmetric, so its geometry is entirely defined by the spinner radius R_1 and the nacelle radius R_2 [27]:

$$\begin{aligned} R_1(x) &= \max\left(0, 0.64212 - \left(0.04777 + 0.98234y^2\right)^{0.5}\right), \\ R_2(x) &= 1 - 0.18453y^2 + 0.10158\frac{\mathrm{e}^{-11(1-y)} - \mathrm{e}^{-11}}{1 - \mathrm{e}^{-11}}, \\ 0 \leq x \leq L,\ & y = x/L \text{ and } L = 2. \end{aligned} \tag{41}$$

The fan is located at the axial position $x = 0$ and the duct exit is at $x = L$. The flow characteristics are specified at the fan location, with a zero or non zero axial velocity and a unit value for both the density and speed of sound. The acoustic source is also specified at the same position and propagates against the flow. Infinite duct conditions are assumed at both ends, which means that they have zero reflection coefficients.

For test cases with a liner, a constant impedance $Z_2 = 2 - \mathrm{i}$ is applied between $x = 0.2$ and $x = 1.8$.

2. Numerical procedure

The method is first evaluated against a method where the axial variation of the acoustic variables is determined analytically. In the case of slowly varying ducts, a leading order approximation of the exact solution can be found using the Wentzel–Kramers–Brillouin (WKB) method when mode transitions (change of mode behaviour from cut-on to cut-off or vice-versa) do not occur. This has been proposed by Rienstra [4] and validated numerically [28]. In the case of single or double transition, other expressions can be derived and are added here to strengthen the comparisons [27, 29, 30]. These first comparisons aim to evaluate the benefit from using the present method instead of an analytical models, noting that the calculation time is similar.

Then, the validation is pursued using a finite-element model (FEM) [31] which computes both the steady potential flow and the acoustic field. The solver is based on a weak formulation of equations (1) and (2) over a volume V bounded by a surface S. In this solver, the lined wall boundary condition is also implemented using the Myers formulation [19]. For the injection/exit boundary conditions, a representation over transverse hard-walled modes is used, which allows to specify the incoming mode and to avoid any spurious reflection on the source/exit plane. Quadratic elements (6 nodes triangles) are used to represent the solutions.

When the FEM is used, two cases can be distinguished. FEM computations are performed using the flow computed with the MS approximation (referred to as FEM/MS) to check that our method is correctly implemented and that the $O(\epsilon^2)$ terms neglected in equation (8) do not impact the solution. Then, FEM solutions that use the complete flow obtained by solving equation (1) (referred to as FEM/CFD) are compared to the MM results. This allows us to understand the limitation brought by the use of a MS flow and the impact of the neglected $O(\epsilon^2\omega^2 U_0)$ terms. It is unlikely that these terms can be neglected at high frequencies when a high-velocity mean flow is used. Typically for frequencies $\omega \sim \epsilon^{-1}$ and high velocities $U_0 \sim 1$, the neglected scattering terms could be, in theory, of the same order of magnitude as one of the computed scattering terms. Note that the error is expected to be equal to numerical precision in all the cases without flow ($M_0 = 0$).

For the MM calculations, two different bases can be applied (see section III.E). The Chebyshev one is preferred since it gives shorter calculation times than the Bessel functions. Nevertheless, the multimodal method is also used with the Bessel basis since the modal scattering can be artificially turn-off (see section III.E). In that case, there is no interaction between modes and their resolution can be dissociated. Therefore, the problem reduces to a scalar integration, which

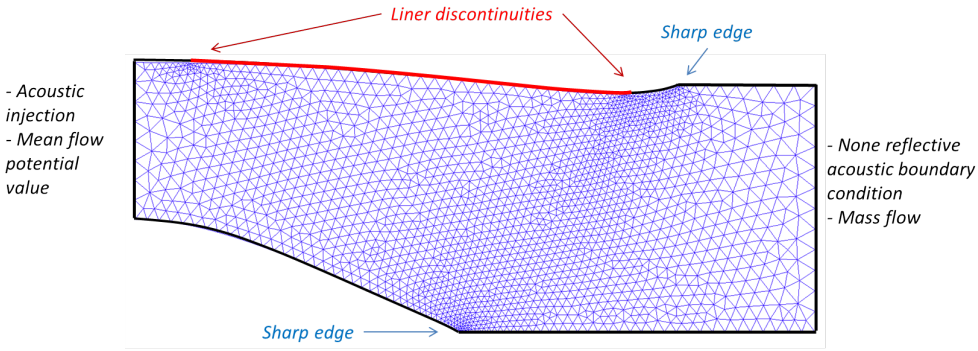

Fig. 4 Visualization of the mesh used when there is a liner (under-meshed for the sake of visibility).

drastically decreases the calculation time. This multimodal method without scattering is referred to as MMWS in the following. Comparisons with the MM results (with Chebyshev basis) allow understanding the improvement brought by a formulation that captures the scattering mechanisms.

3. Numerical details

Details about the numerical resolution are defined here and will be applied to all the test cases. For the developed multimodal method, the Riccati equation for the admittance matrix is integrated using a Magnus-Moebius scheme of order four [32]. The number of basis functions used in the radial direction is $2n + 10$ polynomials, with n the radial order of the injected mode (see section V). For the axial discretization, twenty points per free field wavelength are used. This resolution can be insufficient for highly evanescent modes as it does not correctly recover for their rapid decay but this is not problematic in this paper because the errors related to the multiple-scale assumption are higher. Note that the discretization does not need to be refined near a liner discontinuity since the admittance jump is given by the expression (39).

With these criteria, all the test cases that are presented took less than one second to run with the developed multimodal method.

For the FEM, the acoustic potential field is interpolated on an unstructured, triangular mesh generated using Gmsh [33]. The terminal plane needs to be located far enough from regions of non-uniformities. Therefore, the duct is extended by 0.5 to have an exit condition where the flow can be assumed uniform. A mesh convergence process is carried out to evaluate if the acoustic field is correctly represented. When using the FEM solver, there is also a need to refine the sharp edges and the liner discontinuities to have an accurate solution. An example of a numerical mesh is shown in figure 4.

4. Flow computation

For cases with flow, M_0, C_0 and D_0 values are specified at the axial location of the fan (with $C_0 = 1$ and $D_0 = 1$ in all case). The steady axial velocity and the velocity streamlines obtained with the FEM are represented in figure 5a for a specified Mach number $M_0 = -0.4$. The axial velocity averaged over successive cross-sections is also shown and is compared with the flow computed by the multiple-scales (MS) method (see section II.B) in figure 5b. Even if the averaged axial velocity obtained with both methods is almost identical, there are important radial variations that are not predicted by the MS method ($U = U_0(x) + O(\epsilon^2)$). This is particularly the case near the exit ($x = L$) of the duct where the geometry is not slowly-varying ($\epsilon \approx \mathrm{d}R_2/\mathrm{d}x \approx 0.3$).

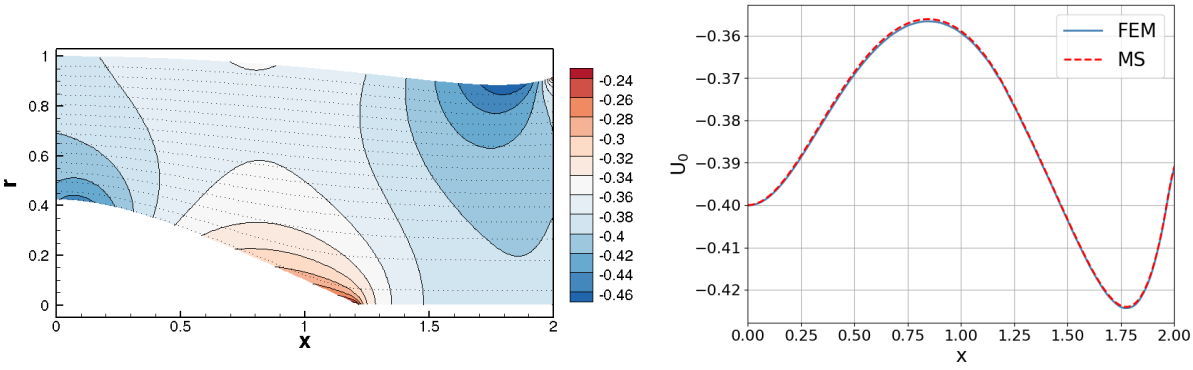

(a) Contours of normalized axial velocity, with the streamlines plotted as dotted black lines

(b) Cross-averaged axial velocity obtained with the FEM solver (solid line) and with the MS approximation (dotted line)

Fig. 5 Flow computed for a specified Mach number $M_0 = -0.4$ at $x = 0$.

B. Hard-walled cases

The intention here is to explore both the model's ability to represent the physics and the numerical stability of the implementation for cases without wall acoustic treatment.

1. Cut-on mode

First, the benefit of using the model is shown at a low frequency ($\omega = 3$) by computing the propagation of the mode $(m, n) = (1, 1)$ for a specified Mach number $M_0 = -0.4$ at the fan level. This is illustrated in figure 6 by comparing the pressure contours over the meridional plane given by the WKB, the MM, the MMWS and the FEM results.

The WKB and the MMWS results are in excellent agreement. In cases where few reflections are expected inside the duct, the two methods give similar results. However, the results of both methods differ from the cases where scattering is accounted for. The agreement between the MM and the FEM/MS is excellent, and the minor differences that can be observed come from the neglected $O(\epsilon^2)$ flow terms in the equation governing the acoustics. The MM results slightly differ from the FEM/CFD ones, and this is to be related to the $O(\epsilon^2\omega^2 U_0)$ scattering terms that have been neglected.

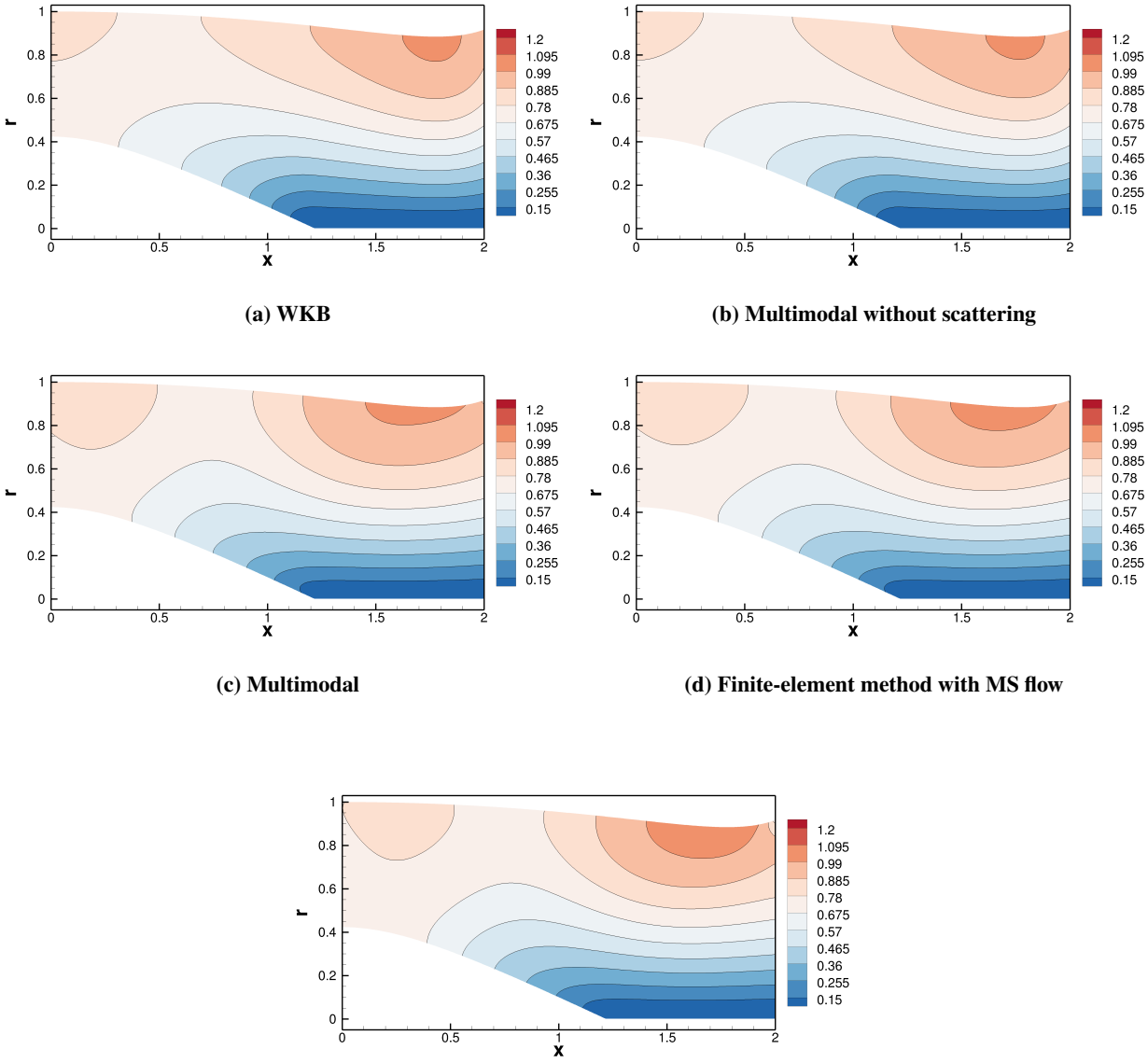

(a) WKB

(b) Multimodal without scattering

(c) Multimodal

(d) Finite-element method with MS flow

(e) Finite-element method with CFD flow

Fig. 6 Pressure magnitude associated to the mode (1,1) at $\omega = 3$ and $M_0 = -0.4$.

Note that the fact that the CFD flow considers a constant duct at the outlet also tends to artificially reduce the radial flow velocity values near the exit, increasing the discrepancies between both methods.

2. Transition mode (cut-on/cut-off)

The stability close to a transition (change of mode behaviour from cut-on to cut-off or vice-versa.), which corresponds to a singularity of the admittance matrix [1], is evaluated by performing the same analysis but at a frequency of $\omega = 31.0$ and for a mode $(m, n) = (20, 3)$. The results are plotted in figure 7. The MMWS and the WKB are in good agreement, which indicates that the Magnus-Moebius scheme avoids numerical instability despite the quasi-singularity of the admittance matrix and can capture total reflection phenomena, such as the ones obtained at the axial location of turning points. Note that this means that any number of transition and near transition phenomena can be captured without the need to modify the model. This makes the MMWS typically suited to study amplification or resonance caused by trapped modes (see [30]). In this case, the inclusion of modal scattering and of a complete flow is not significant as all the methods give similar results.

3. Frequency evolution

In order to evaluate more precisely the accuracy of all the methods, we compute the evolution of the error as the frequency and flow velocity increase for three different modes: $(m, n) = (1, 1)$, $(m, n) = (20, 1)$ and $(m, n) = (20, 3)$. The error is evaluated using the L^2 norm:

$$\mathcal{E} = \left(\frac{\int_0^L \int_{R_1}^{R_2} |\phi - \phi_\infty|^2 r \mathrm{d}r\mathrm{d}x}{\int_0^L \int_{R_1}^{R_2} |\phi_\infty|^2 r \mathrm{d}r\mathrm{d}x} \right)^{1/2}, \tag{42}$$

with ϕ the potential obtained with the MM, the MMWS and the WKB method, and ϕ_∞ the reference FEM solution (Using a L^2 norm instead of a L^1 norm is penalizing but is kept for coherence with section V).

The results obtained when using the FEM/MS as reference solution are given in figure 8.

Given the approximations of the method, there is a good quantitative agreement between the MM formulation and the FEM/MS, with discrepancies always inferior to 10% (of order $O(\epsilon^2)$). If the expected flow is close to the MS flow, the MM method will give accurate results in a calculation time almost identical to a semi-analytical model. The scattering and convection effects of this flow are encapsulated without deteriorating the computational efficiency of standard multimodal methods.

The results obtained when the FEM/CFD is used as the reference solution and compared to the MM, the MMWS and the WKB method are plotted in figure 9.

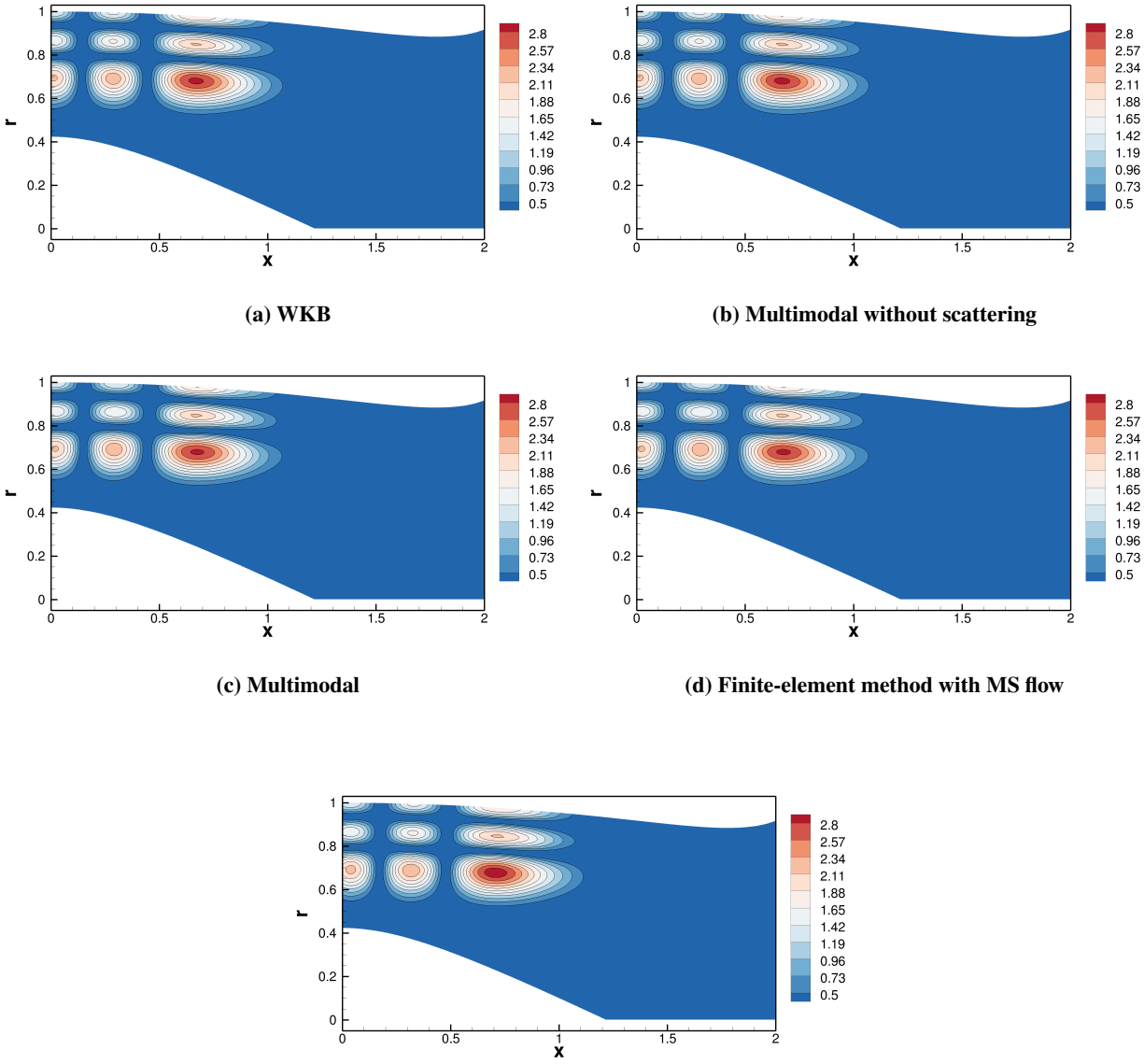

(a) WKB

(b) Multimodal without scattering

(c) Multimodal

(d) Finite-element method with MS flow

(e) Finite-element method with CFD flow

Fig. 7 Pressure magnitude associated to the mode (20,3) at $\omega = 31$ and $M = -0.4$.

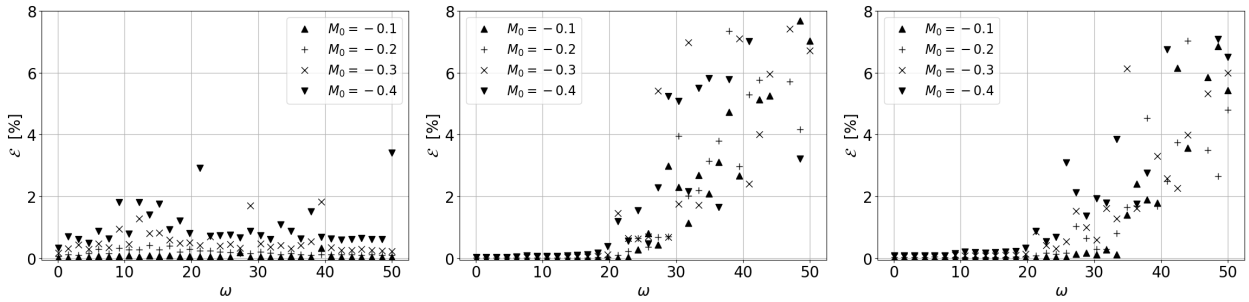

(a) $(m, n) = (1, 1)$ **(b)** $(m, n) = (20, 1)$ **(c)** $(m, n) = (20, 3)$

Fig. 8 Relative error between the FEM/MS as the reference solution and the MM method, for various flows and frequencies.

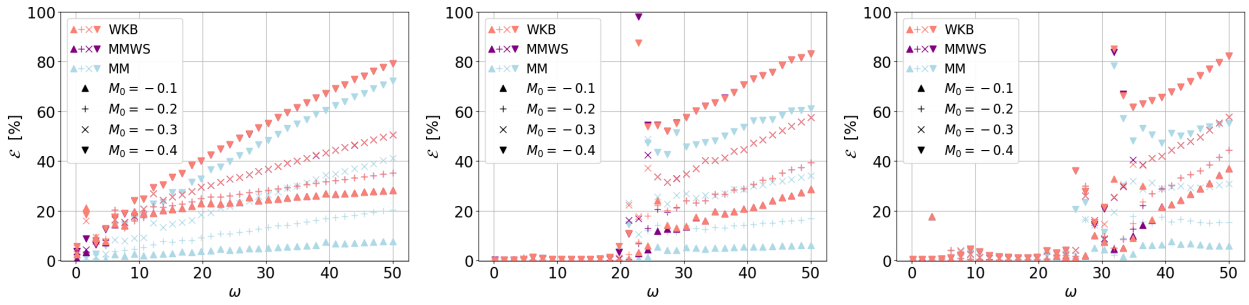

(a) $(m, n) = (1, 1)$ **(b)** $(m, n) = (20, 1)$ **(c)** $(m, n) = (20, 3)$

Fig. 9 Relative error between the FEM/CFD as the reference solution and the MM, the MMWS and the WKB method, for various flows and frequencies.

A key observation from the comparison between the FEM/CFD and MMWS results and the FEM/CFD and WKB results is that the MMWS and WKB method are equivalent in both cut-off and cut-on regions. The only region where the two methods differ is where reflection phenomena can occur typically near transition regions [34]. When the FEM/CFD results are compared to the MM results, the agreement is still excellent for low flow velocities where the MM model is particularly suited. However when strong flow velocities are used, the agreement deteriorates, especially for high frequencies. Even if the evolution of the errors is highly dependent on the mode injected, some general trends are visible for the three computed cases:

- In regions where the mode is cut-on (approximately $\omega > m$), the error increases with the frequency and flow velocity. The distance to the transition region mainly drives this error. Therefore the increase of the azimuthal mode order is favourable to the model.
- In regions where the mode is cut-off, the MM results perfectly fit the FEM results. The model captures the high attenuation of the mode. For this case, there is few scattering, which explains the observed agreement.
- The results deteriorate when the mode encounters at least one transition in the duct. This comes from the fact that transitions are very sensitive to small parameter changes so that even a minute error on the flow can change the response of the overall system [27].

C. Lined wall cases

Eight test cases are used to validate the capability of the model to predict sound attenuation in lined turbofan inlets. Since the transverse mode differs before and after the liner, the models that neglect the scattering cannot be used here. Therefore only the MM and the FEM can represent the propagation in such a duct.

The validation is shown in terms of the power attenuation predicted by each method, defined by:

$$\Delta P = 10 \log_{10} \left(\frac{P_{source}}{P_{exit}} \right), \tag{43}$$

where P_{source} and P_{exit} refer to the acoustic power at the source plane and the exit plane respectively.

1. No-flow cases

The first test cases are done without flow where we expect the MM model to be perfectly accurate. The attenuation obtained with our method and both FEM computations is given for all the test cases in table 1. All the methods agree and the model appears to be a powerful tool to compute an estimated attenuation.

Case	(m,n)	ω	MM	FEM/MS	FEM/CFD
1	(10,1)	16	44.1 dB	44.1 dB	44.1 dB
2	(12,1)	20	47.5 dB	47.5 dB	47.5 dB
3	(20,7)	44.5	24.5 dB	24.5 dB	24.5 dB
4	(30,2)	50	21.8 dB	21.8 dB	21.8 dB

Table 1 Summary of the lined test case parameters and results for $M_0 = 0$.

2. Flow cases

Then test cases are done with a specified Mach number $M_0 = -0.4$. Here the model should give approximate results. The attenuation obtained are summarised in table 2.

Case	(m,n)	ω	MM	FEM/MS	FEM/CFD	$\Delta(MM - FEM/CFD)$
1	(10,1)	16	49.7 dB	50.1 dB	49.0 dB	0.7dB
2	(12,1)	20	25.3 dB	25.1 dB	24.8 dB	0.5dB
3	(20,7)	44.5	30.7 dB	28.9 dB	31.9 dB	-1.2dB
4	(30,2)	50	14.3 dB	15.5 dB	14.0 dB	0.3dB

Table 2 Summary of the lined test case parameters and results for $M_0 = -0.4$.

Discrepancies appear between all methods (even the FEM/MS and MM results differ) and no global trend appears. Nevertheless, the MM still estimates the expected attenuation correctly and the prediction rarely differs by more than 1dB from the reference FEM/CFD results.

To understand the slight difference predicted by all the methods, pressure plots associated with test case 4 are shown in figure 10. We first notice a good agreement regarding pressure contours and that the junction condition proposed for the admittance gives consistent results. As expected by the formulation derived in section IV, there is a reflection at the axial location of the liner discontinuity (visible at $x = 0.2$). Even if the impact of the liner is overestimated with the MM method, no major contrasts are observed. The flow-induced scattering phenomena are of an order of magnitude inferior to the impact of the liner, and the attenuation predicted by our model is accurate.

VII. Conclusion

In this paper, a multimodal method for the computation of the acoustic field in an axisymmetric duct with a multiple scales potential mean flow has been developed. The acoustic problem has been solved by transforming the acoustic potential equation into a set of coupled one-dimensional equations on the amplitude of base functions. A procedure has also been added to deal with liner discontinuity. The method uses two basis types: one based on Chebyshev polynomials, which proved to be effective at solving the wall boundary condition issue of most multimodal methods and allows for fast

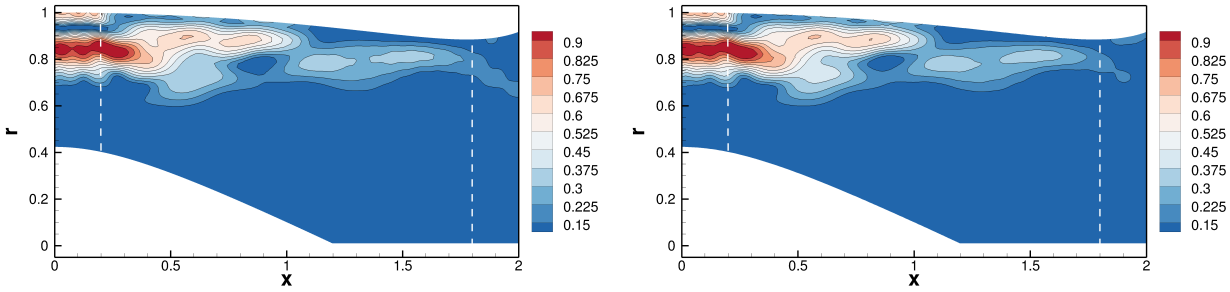

(a) Multimodal

(b) Finite-element method with MS flow

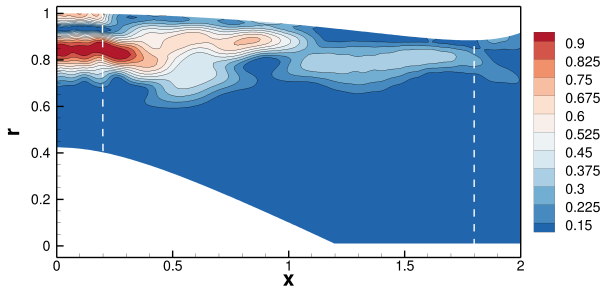

(c) Finite-element method with CFD flow

Fig. 10 Pressure magnitude associated to the mode (30,2) at $\omega = 50$ for $M = -0.4$ and $Z_2 = 2 - \mathrm{i}$.

calculations; and the other based on Bessel functions, which allows to dissociate the self-propagation of modes from the scattering phenomena. When a Chebyshev basis is used, the method is very efficient because all the radial integrations of the multimodal formulation are independent of the frequency, the flow, the geometry and the azimuthal order.

Comparisons with a WKB method, a finite-element method which uses the same approximate flow, and one which uses a complete flow, have been carried out for a model of a turbofan inlet duct over a large range of flows and frequencies. The comparisons were made on pressure contours for the hard-walled test cases, and on power attenuation for the lined-wall ones. The agreement between the proposed multimodal method and the FEM that uses an approximate flow is excellent in most cases, but it deteriorates for high frequencies and Mach numbers when compared to the FEM that uses a complete flow. Therefore, improving the flow representation would be necessary since some flow-induced scattering are not present when using the multiple-scales approximation for the flow. Still, the present multimodal formulation appears very efficient for studying propagation inside realistic turbofan engine inlets. In particular, the error made by our model is always inferior to the one made by the WKB method which neglects the modal scattering.

The efficiency and numerical cost can be improved drastically by parallelizing the axial integration, but this appeared not to be necessary for a 2D geometry, with all the test cases running in less than one second. This paper demonstrates the efficiency of the multimodal method which allows to compute acoustic propagation inside lined ducts with simplified potential flows without additional cost when compared to no-flow multimodal methods.

A. Multimodal matrices formulation when the Fourier-Chebyshev basis is used

By introducing:

$$I_k(f,g) = \int_0^1 f(r)g(r)r^k \mathrm{d}r, \tag{44}$$

and the symbol $'$ to represent the first derivative of the Chebyshev polynomial, the matrices defined in equation (14) write:

$$
\begin{aligned}
\mathcal{A}_{ij} &= 2\pi\left((R_2-R_1)^2 I_3(T_i,T_j) + 3(R_2-R_1)R_1 I_2(T_i,T_j) + 3R_1^2 I_1(T_i,T_j) + \frac{R_1^3}{R_2-R1} I_0(T_i,T_j)\right),\\
\mathcal{B}_{ij} &= 2\pi\left(-\frac{1}{R_2-R1}\frac{\mathrm{d}(R_2-R_1)}{\mathrm{d}X}\mathcal{A}_{ij} - (R_2-R_1)\frac{\mathrm{d}(R_2-R_1)}{\mathrm{d}X} I_4(T_i,T_j') + \left(4R_1\frac{\mathrm{d}R_1}{\mathrm{d}X} - 3\frac{\mathrm{d}R_2}{\mathrm{d}X}R_1 - R_2\frac{\mathrm{d}R_1}{\mathrm{d}X}\right) I_3(T_i,T_j')\right.\\
&\quad - \left(\frac{3R_1^2}{R_2-R1}\frac{\mathrm{d}(R_2-R_1)}{\mathrm{d}X} + 3R_1\frac{\mathrm{d}R_1}{\mathrm{d}X}\right) I_2(T_i,T_j') - \left(\frac{R_1^3}{(R_2-R_1)^2}\frac{\mathrm{d}(R_2-R_1)}{\mathrm{d}X} + \frac{3R_1^2}{R_2-R1}\frac{\mathrm{d}R_1}{\mathrm{d}X}\right) I_1(T_i,T_j')\\
&\quad \left. - \frac{R_1^3}{(R_2-R_1)^2}\frac{\mathrm{d}R_1}{\mathrm{d}X} I_0(T_i,T_j')\right),\\
C_{ij} &= 2\pi\frac{V^a}{C}\left(\mathcal{A}_{ij} + (R_2-R_1)^2 I_4(T_i,T_j') + 4(R_2-R_1)R_1 I_3(T_i,T_j') + 6R_1^2 I_2(T_i,T_j')\right.\\
&\quad \left. + \frac{4R_1^3}{R_2-R_1} I_1(T_i,T_j') + \frac{R_1^4}{(R_2-R_1)^2} I_0(T_i,T_j')\right)\\
&\quad + 2\pi\frac{V^b}{C}\left(I_1(T_i,T_j) + \frac{R_1}{R_2-R_1} I_0(T_i,T_j) + I_2(T_i,T_j') + \frac{2R_1}{R_2-R_1} I_1(T_i,T_j') + \frac{R_1^2}{(R_2-R_1)^2} I_0(T_i,T_j')\right),\\
\mathcal{D}_{ij} &= \frac{2\pi}{R_2-R_1}\left((R_2-R_1)(1+m^2) I_1(T_i,T_j) + R_1(1+m^2) I_0(T_i,T_j) + (R_2-R_1)(I_2(T_i,T_j') + I_2(T_i,T_j')^*) + \right.\\
&\quad 2R_1(I_1(T_i,T_j') + I_1(T_i,T_j')^*) + \frac{R_1^2}{R_2-R_1}(I_0(T_i,T_j') + I_0(T_i,T_j')^*) + (R_2-R_1) I_3(T_i',T_j') + 3R_1 I_2(T_i',T_j')\\
&\quad \left. + \frac{3R_1^2}{R_2-R_1} I_1(T_i',T_j') + \frac{R_1^3}{(R_2-R_1)^2} I_0(T_i',T_j')\right),
\end{aligned}
\tag{45}
$$

when $m \neq 0$ and:

$$
\begin{aligned}
\mathcal{A}_{ij} &= 2\pi\left((R_2-R_1)^2 I_1(T_i,T_j) + R_1(R_2-R_1) I_0(T_i,T_j)\right),\\
\mathcal{B}_{ij} &= 2\pi\left(-(R_2-R_1)\frac{\mathrm{d}(R_2-R_1)}{\mathrm{d}X} I_2(T_i,T_j') + \frac{\mathrm{d}\left(R_1^2 - R_2R_1\right)}{\mathrm{d}X} I_1(T_i,T_j') - R_1\frac{\mathrm{d}R_1}{\mathrm{d}X} I_0(T_i,T_j')\right),\\
C_{ij} &= 2\pi\frac{V^a}{C}\left((R_2-R_1)^2 I_2(T_i,T_j') + 2R_1(R_2-R_1) I_1(T_i,T_j') + R_1^2 I_0(T_i,T_j')\right)\\
&\quad + 2\pi\frac{V^b}{C} I_0(T_i,T_j'),\\
\mathcal{D}_{ij} &= 2\pi\left(I_1(T_i',T_j') + \frac{R_1}{R_2-R_1} I_0(T_i',T_j')\right),
\end{aligned}
\tag{46}
$$

when $m = 0$.

Acknowledgments

ONERA carried out these activities in the framework of the ADEC project. This project has received funding from the Clean Sky 2 Joint Undertaking within the European Union's Horizon 2020 research and innovation program, under

grant agreement GA ID No. 945583 - LPA IADP 2020-2021.

References

[1] Pagneux, V., "Multimodal admittance method in waveguides and singularity behavior at high frequencies," *Journal of Computational and Applied Mathematics*, Vol. 234, No. 6, 2010, pp. 1834–1841. https://doi.org/10.1016/j.cam.2009.08.034.

[2] Gabard, G., "Noise sources for duct acoustics simulations: Broadband noise and tones," *AIAA Journal*, Vol. 52, No. 9, 2014, pp. 1994–2006. https://doi.org/10.2514/1.J052739.

[3] Goldstein, M. E., *Aeroacoustics*, McGraw-Hill International Book Company, 1976.

[4] Rienstra, S. W., "Sound transmission in slowly varying circular and annular lined ducts with flow," *Journal of Fluid Mechanics*, Vol. 380, 1999, pp. 279–296. https://doi.org/10.2514/6.1998-2311.

[5] Cooper, A. J., and Peake, N., "Propagation of unsteady disturbances in a slowly varying duct with mean swirling flow," *Journal of Fluid Mechanics*, Vol. 445, 2001, pp. 207–234. https://doi.org/10.1017/s0022112001005559.

[6] Peake, N., and Cooper, A. J., "Acoustic propagation in ducts with slowly varying elliptic cross-section," *Journal of Sound and Vibration*, Vol. 243, No. 3, 2001, pp. 381–401. https://doi.org/10.1006/jsvi.2000.3411.

[7] Brambley, E. J., and Peake, N., "Sound transmission in strongly curved slowly varying cylindrical ducts with flow," *Journal of Fluid Mechanics*, Vol. 596, 2008, pp. 387–412. https://doi.org/10.1017/S0022112007009603.

[8] Rienstra, S. W., "Slowly varying modes in a two-dimensional duct with shear flow and lined walls," *Journal of Fluid Mechanics*, Vol. 906, 2020. https://doi.org/10.1017/jfm.2020.687.

[9] "Actran 15 User's Guide, vols1,2," , 2014.

[10] Achunche, I., Astley, J., Sugimoto, R., and Kempton, A., "Prediction of forward fan noise propagation and radiation from intakes," *15th AIAA/CEAS Aeroacoustics Conference (30th AIAA Aeroacoustics Conference)*, 2009. https://doi.org/10.2514/6.2009-3239.

[11] Astley, R. J., Sugimoto, R., and Mustafi, P., "Computational aero-acoustics for fan duct propagation and radiation. Current status and application to turbofan liner optimisation," *Journal of Sound and Vibration*, Vol. 330, No. 16, 2011, pp. 3832–3845. https://doi.org/10.1016/j.jsv.2011.03.022.

[12] Prinn, A. G., Sugimoto, R., and Astley, R. J., "The effect of steady flow distortion on noise propagation in turbofan intakes," *22nd AIAA/CEAS Aeroacoustics Conference, 2016*, 2016. https://doi.org/10.2514/6.2016-3028.

[13] Smith, A. F., Ovenden, N. C., and Bowles, R. I., "Flow and geometry induced scattering of high frequency acoustic duct modes," *Wave Motion*, Vol. 49, No. 1, 2011, pp. 109–124. https://doi.org/10.1016/j.wavemoti.2011.07.006.

[14] Wilson, A., "Propagation of acoustic perturbations in non-uniform ducts with non-uniform mean flow using eigen analysis in general curvilinear coordinate systems," *Journal of Sound and Vibration*, Vol. 443, 2019, pp. 605–636. https://doi.org/10.1016/j.jsv.2018.11.023.

[15] Pagneux, V., Amir, N., and Kergomard, J., "A study of wave propagation in varying cross-section waveguides by modal decomposition. Part I. Theory and validation," *The Journal of the Acoustical Society of America*, Vol. 100, No. 4, 1996, p. 2034. https://doi.org/10.1121/1.417913.

[16] Lu, Y. Y., "A fourth-order Magnus scheme for Helmholtz equation," *Journal of Computational and Applied Mathematics*, Vol. 173, No. 2, 2005, pp. 247–258. https://doi.org/10.1016/j.cam.2004.03.010.

[17] Félix, S., and Pagneux, V., "Multimodal analysis of acoustic propagation in three-dimensional bends," *Wave Motion*, Vol. 36, No. 2, 2002, pp. 157–168. https://doi.org/10.1016/S0165-2125(02)00009-4.

[18] Guennoc, T., Doc, J. B., and Félix, S., "Improved multimodal formulation of the wave propagation in a 3D waveguide with varying cross-section and curvature," *The Journal of the Acoustical Society of America*, Vol. 149, No. 1, 2021, pp. 476–486. https://doi.org/10.1121/10.0003336.

[19] Ingard, U., "Influence of Fluid Motion Past a Plane Boundary on Sound Reflection, Absorption, and Transmission," *The Journal of the Acoustical Society of America*, Vol. 31, No. 7, 1959, pp. 1035–1036. https://doi.org/10.1121/1.1907805.

[20] McTavish, J. P., and Brambley, E. J., "Nonlinear sound propagation in two-dimensional curved ducts: A multimodal approach," *Journal of Fluid Mechanics*, Vol. 875, 2019, pp. 411–447. https://doi.org/10.1017/jfm.2019.497.

[21] Canuto, C., Houssanini, M. Y., Quarteroni, A., and Zang, T. A., *Springer series in computational physics*, Springer, New York, 1988. https://doi.org/10.1016/0010-4655(84)90059-6.

[22] Boyer, G., Piot, E., and Brazier, J. P., "Theoretical investigation of hydrodynamic surface mode in a lined duct with sheared flow and comparison with experiment," *Journal of Sound and Vibration*, Vol. 330, No. 8, 2010, pp. 1793–1809. https://doi.org/10.1016/j.jsv.2010.10.035.

[23] Ralph Lewis, H., and Bellan, P. M., "Physical constraints on the coefficients of Fourier expansions in cylindrical coordinates," *Journal of Mathematical Physics*, Vol. 31, No. 11, 1990, pp. 2592–2596. https://doi.org/10.1063/1.529009.

[24] Gabard, G., and Astley, R. J., "A computational mode-matching approach for sound propagation in three-dimensional ducts with flow," *Journal of Sound and Vibration*, Vol. 315, No. 4-5, 2008, pp. 1103–1124. https://doi.org/10.1016/j.jsv.2008.02.015.

[25] Eversman, W., "The boundary condition at an impedance wall in a non-uniform duct with potential mean flow," *Journal of Sound and Vibration*, Vol. 246, No. 1, 2001, pp. 63–69. https://doi.org/10.1006/jsvi.2000.3607.

[26] Astley, R. J., Sugimoto, R., Gabard, G., Norde, E., Grift, E. J., and Bocquier, M., "The effect of steady flow distortion on mode propagation in a turbofan intake," *20th AIAA/CEAS Aeroacoustics Conference*, 2014. https://doi.org/10.2514/6.2014-3113.

[27] Ovenden, N. C., Eversman, W., and Rienstra, S. W., "Cut-on cut-off transition in flow ducts: comparing multiple-scales and finite-element solutions," *10th AIAA/CEAS Aeroacoustics Conference*, 2004. https://doi.org/10.2514/6.2004-2945.

[28] Rienstra, S. W., and Eversman, W., "A numerical comparison between multiple-scales and finite-element solution for sound propagation in lined flow ducts," *Journal of Fluid Mechanics*, Vol. 437, 2001, pp. 367–384. https://doi.org/10.2514/6.1999-1821.

[29] Ovenden, N. C., "A uniformly valid multiple scales solution for cut-on cut-off transition of sound in flow ducts," *Journal of Sound and Vibration*, Vol. 286, No. 1-2, 2005, pp. 403–416. https://doi.org/10.1016/j.jsv.2004.12.009.

[30] Mangin, B., Daroukh, M., and Gabard, G., "An application of the multiple-scales theory to acoustic double transition in ducts with flow," *Journal of Sound and Vibration*, Vol. 539, 2022. https://doi.org/10.1016/j.jsv.2022.117252.

[31] Gabard, G., "PFE Software," , 2021. URL https://github.com/GwenaelGabard/pfe.

[32] Iserles, A., Marthinsen, A., and Nørsett, S. P., "On the implementation of the method of magnus series for linear differential equations," *BIT Numerical Mathematics*, Vol. 39, No. 2, 1999, pp. 281–304. https://doi.org/10.1023/A:1022393913721.

[33] Geuzaine, C., and Remacle, J. F., "Gmsh: A 3-D finite element mesh generator with built-in pre-and post-processing facilities," *International journal for numerical methods in engineering*, Vol. 79, No. 11, 2009, pp. 1309–1331. https://doi.org/10.1002/nme.2579.

[34] Nielsen, R. B., and Peake, N., "Tunnelling effects for acoustic waves in slowly varying axisymmetric flow ducts," *Journal of Sound and Vibration*, Vol. 380, 2016, pp. 180–191. https://doi.org/10.1016/j.jsv.2016.06.003.